ELSEVIER

International Journal of Mass Spectrometry 206 (2001) 63–78

International Journal of Mass Spectrometry

Observation of multiply charged cluster anions upon pulsed UV laser ablation of metal surfaces under high vacuum

Carsten Stoermer, Jochen Friedrich, Manfred M. Kappes*

Institut für Physikalische Chemie, Universität Karlsruhe, Kaisestrasse 12, 76128 Karlsruhe, Germany

Received 22 August 2000; accepted 4 October 2000

Abstract

Pulsed N_2-laser ablation of various metal targets (M=Au, Pb, Pt, Bi, Sb) in high vacuum gives rise to series of neutral as well as singly positively and negatively charged clusters. Largest clusters, ranging in size to >100 atoms, were seen for gold and lead targets. For these metals, mass spectral signal-to-noise ratio was sufficient to also observe a series of doubly negatively charged clusters, Pb_x^{2-} and Au_x^{2-}—commencing at threshold sizes of 35 and 29, respectively. In the case of lead, triply negatively charged clusters (Pb_x^{3-}, $x > 76$) were also detected. Multianion threshold sizes result from the metastable decay of hot clusters and are associated with a size-dependent transition from evaporation (i.e., neutral atom loss) to electron autodetachment for smaller cluster sizes. (Int J Mass Spectrom 206 (2001) 63–78) © 2001 Elsevier Science B.V.

Keywords: Metal clusters; Laser ablation; Multiply negatively charged ions

1. Introduction

With the recent advent of suitably intense ion sources, multiply negatively charged gas-phase molecular ions (multianions) have become of great interest [1]. As an example, it has recently proven possible to spectroscopically characterize several isolated transition metal tetrahalide dianions (MX_4^{2-}; M=Pd, Pt; and X=Cl, Br). At five atoms, these are the smallest dianions so far known to be (meta)stable on a mass spectroscopic time scale [2]. It has been shown by a combination of quantum chemistry, photoelectron spectroscopy, and direct measurements of the decay rate that specific MX_4^{2-}, notably $PtCl_4^{2-}$, are metastable with regard to both halide and electron loss [2,3]. Such metastability is associated with Coulomb barriers that need to be surmounted (or, for electron loss, tunneled through) for decay into two (singly) negatively charged particles to occur.

Like MX_4^{2-}, most multianions now known in gas-phase have been generated by electrospraying from the appropriate polar solution [1]. While electrospraying can even be used to make stoichiometric alkali halide salt-cluster multianions out of salt solutions [4], such a source is not compatible with the formation of elemental cluster multianions. Furthermore, while the atomic vapor expansion sources commonly applied to making bare clusters of the more refractory elements (laser vaporization [5], PACIS [6], and gas aggregation [7]) can be readily modified to generate cluster monoanions, negatively charged clusters in higher charged states have so far

* Corresponding author. E-mail: manfred.kappes@chemie.uni-karlsruhe.de

PII S1387-3806(00)00390-0

proven inaccessible. In fact, until recently the only known such species were a series of oxygen cluster dianions generated by electron pickup onto neutral O_2 clusters [8], a number of small carbon cluster dianions formed by Cs^+ ion sputtering of graphite [9], as well as several fullerene dianions, which were first generated by laser ablation/ionization [10,11].

In a pioneering study, Schweikhard et al. have recently succeeded in making long-lived (>1 s) doubly and later triply negatively charged clusters of a variety of transition metals, notably gold [12,13] and titanium [14]—starting with mass-selected, thermalized monoanions and adding one or more low-energy electrons to the ions stored in a Penning trap. In this article, we present a simpler laser ablation approach to making metal cluster multianions—at least for certain heavy metals. Nanosecond-pulsed laser ablation of metal surfaces under high-vacuum conditions is known to give rise to limited cluster formation [15,16]. In addition to neutral clusters, both directly formed singly positively and negatively charged species have been observed with the largest clusters detected, containing ~50 atoms [15,16]. Here we show that laser ablation can also result in a series of doubly and triply negatively charged metal cluster ions in spite of the high vibrational excitation levels initially involved. The mass spectra obtained show characteristic threshold sizes above which multianions occur. We discuss possible formation mechanisms and interpret the threshold sizes in terms of the prevalent metastable decay channels.

2. Experimental

2.1. Overview

Species generated as a result of metal target laser ablation were probed by time-of-flight mass spectroscopy (TOFMS) via both direct extraction of ensuing cations/anions and detection of neutrals via postionization. A 1.8-m-drift-length linear TOFMS equipped with a two-stage throw out mass gate was utilized. The apparatus is shown schematically in Fig. 1a, 1b. Certain aspects of this setup have been described previously [17]. Metal targets were inserted into the first stage of a three-stage, four-plate ion source (repeller [R], extractor [E1, +9 mm relative to the repeller], plate 3 [E2, +9 mm], and plate 4 [B +7 mm], subsequently pumped to a pressure of 10^{-7} mbar and irradiated with a focused N_2 laser (LTB MSG 405 TD, 45° angle of incidence, 100 μm by 200 μm elliptical focus, <13 μJ pulse energy, 500 ps pulse width, and 10 Hz repetition rate). Typically, the higher the ablation laser fluence, the larger the detectable clusters. Consequently, mass spectra were acquired at maximal ablation fluence where possible. To reduce pitting, the target was rotated between laser pulses (~0.2 radians per pulse with the laser focus typically 2 mm from the rotation axis = drift tube axis). Metals were obtained from commercial sources. Their purities were >99.9% for all elements probed.

Several different TOFMS ion-source configurations were used depending on charge state of interest. These are shown schematically in Fig. 2. First, for studies of promptly generated cations, the repeller was maintained at high voltage (typically 10 kV) and the extractor, as well as plates 3 and 4, was grounded. Ions were then immediately accelerated on formation. At the potentials applied, this means that cations clear the ion source and are accelerated up to drift velocity within 500–1000 ns of the laser pulse. This setup yielded the largest cation cluster signals for all metals.

Second, for anion detection, a delayed extraction sequence was applied. Specifically, the repeller-extractor region was initially maintained under nearly field-free conditions with a small retarding potential of ~100 V applied (typically: repeller −10 kV; extractor −10.1 kV for t = 0–5 μs after the ablation pulse). After 5 μs, an acceleration pulse was applied to the repeller (typically: repeller −11 kV, extractor −10.1 kV for t > 5 μs). This procedure limited photoelectron-induced discharges, thus allowing for higher ablation fluences while preventing fast light anions from leaving the source region before the extraction pulse. The delay of 5 μs was found to provide the best anion cluster signal-to-noise ratio (cf. variation in μs steps from 0 to 10 μs) for lead targets. It was not systematically varied for the other targets in this study.

Third, ensuing neutral clusters were characterized

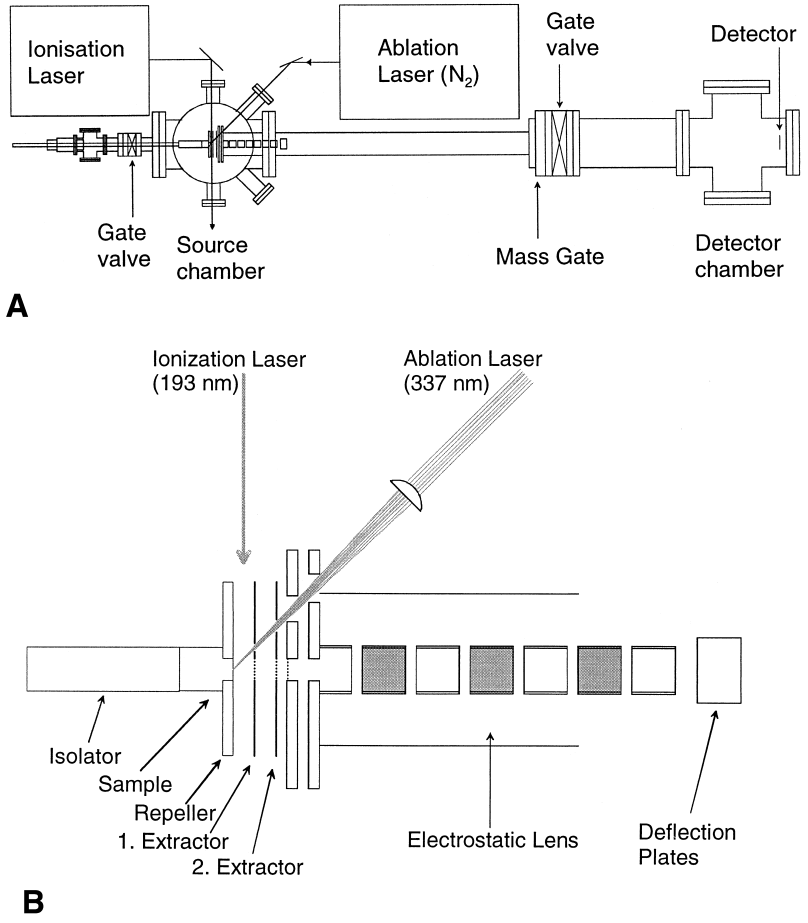

Fig. 1. (*a*) Overview schematic of the experimental apparatus; (*b*) detail of four-stage ion source.

by photoionization using a 193-nm ArF laser pulse (ATL, ATLEX SP 50, 6 mJ pulse energy, 6 mm beam diameter, 3 ns pulselength) propagating between repeller and extractor plates. Typically a delay of 1 μs between ablation and photoionization pulse was used. The ion source was configured in standard Wiley-McLaren fashion (repeller: 20 kV, extractor: 18.9 kV and plate 3: 0V). Information on neutral cluster velocity distributions (see below) was obtained by determining one-photon ionization mass spectra at various ablation/ionization delays.

A number of experiments were performed to test for electric-field dependence of cluster formation. These included: detecting promptly formed cations with a Wiley-McLaren setup (corresponding to an applied electric field of 1 kV/cm during ablation vs. the 10 kV/cm typically applied under the conditions of the first setup) as well as acquiring direct cation mass spectra using initially field-free ion source conditions and an extraction delay analogous to the sequence described above for anion detection. In no case did we observe significant changes to the cluster size distributions as a result of these parameter variations, other than reductions in mass resolution and signal-to-noise ratio.

2.2. Ion focusing lenses, mass gate, and detection

Ions exiting the source region encountered a seven-element lens assembly that focuses them onto a

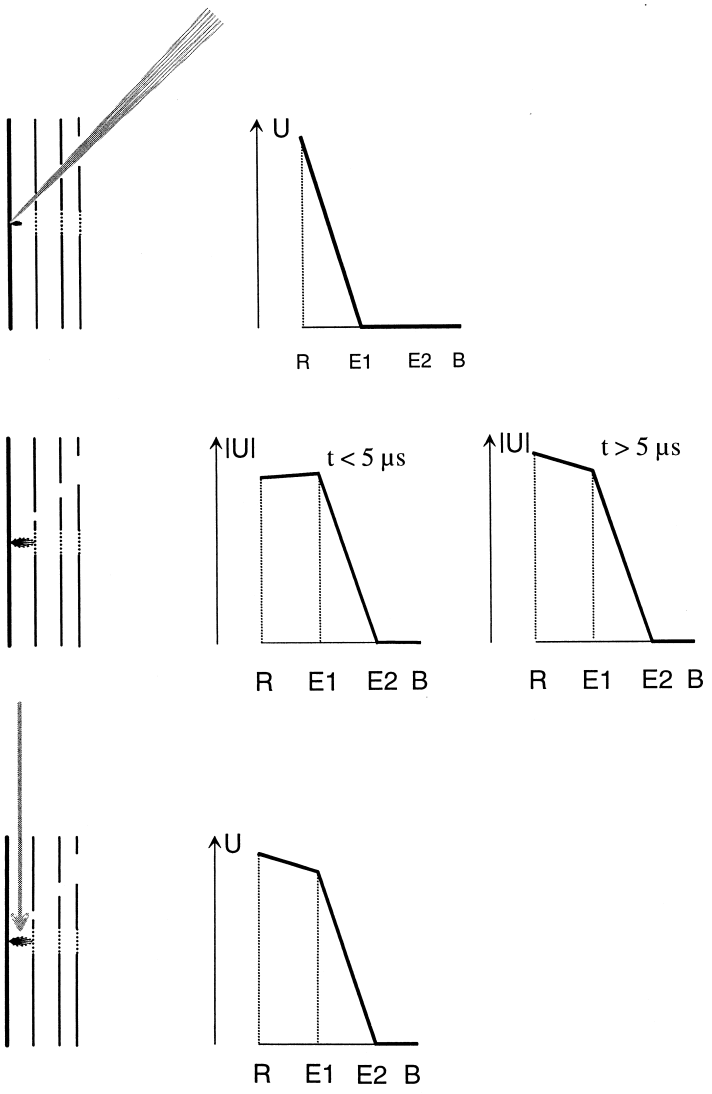

Fig. 2. Ion source configurations used for detection of directly formed cations, anions (delayed extraction), and neutrals (postionization). See text for details.

detector located 1.8 m downstream. For the mass spectroscopic studies presented here, we generally made use of a dual chevron multichannelplate (MCP) detector assembly and acquired the output signal either with a 1-Gs/s digital oscilloscope (large signals) or a 2-ns-channel-width multichannel scaler (small signals). For sensitive detection of a particular cation mass range, the detector was rapidly ramped (200 ns risetime) from a default setting of −1800 V to maximum operating voltage (−2200 V). Anions were detected without MCP ramping.

To obtain a measure of absolute ion fluxes, we also used a fast charge-sensitive detector (CSD) [18]. In particular, ions incident on the CSD encounter a 90% transmission biasable grid before hitting the active detector area. This serves the purpose of preventing the escape of secondary electrons and secondary anions emitted from the active surface.

On their way to the detector, ions transit a double mass gate, which is located 0.8 m upstream from the latter. This has been described in detail in a previous publication [17]. To study metastable decay into neutral and charged products, the mass gate can be set to specific blocking potentials that deflect the corresponding ions from the detector. As we have shown previously, assuming that the ion packet of interest does not fragment before selection, the throwout discrimination of one such mass gate is to first order only a function of the ratio of acceleration to deflection voltage and not of *m/z*. Consequently, all parent *m/z*'s may be removed from the ion beam above a given applied deflection voltage. Using both mass gates in series, we were able to obtain typical discriminations of 99.9% (i.e., 99.9% of nonfragmenting incident ions were deflected outside of the detector active area with a suitable blocking potential applied).

A unique feature of the experimental setup used was its good sensitivity for high-*m/z* species. Apart from the comparatively high MCP incident ion velocities used, this was primarily accomplished by reducing saturation of individual MCP channels as a result of the earlier impact of (more abundant) low-*m/z* clusters and molecules. This was achieved via mass gating light (abundant) ions and, for cations, by (up)pulsing the MCP detector voltage after incidence of residual light ions. Following, we will regard a particular *m/z* species as observed if the corresponding measurement shows a signal-to-noise ratio $S/N \geq 2$.

3. Results

3.1. Neutral and singly charged clusters: mass spectra

3.1.1. Gold

Fig. 3 shows typical mass spectra of prompt gold cluster cations (a), cluster anions (b), and (postionized) cluster neutrals (c), generated on laser ablation of a polycrystalline gold target. Each measurement was obtained by integrating >10,000 individual laser shots. As discussed in section 2.2., single shot measurements were acquired under conditions in which the lighter ions were discriminated against so as not to swamp the MCP detector. Without such discrimination, atoms, dimers, and trimers are dominant for all three charge states.

Anion and neutral mass spectra reflect the composition of the ablated material at the extraction delay (μs), while cation mass spectra are a measure of species present within 100 ns of the laser pulse. Note that postionized neutral cluster size distributions reflect cluster size-dependent ionization potentials (some of which are above the [one] photon energy [19]) folded with unknown vibrational excitation. Consequently, neutral mass spectra are only a rough measure of neutral cluster abundance.

Beyond ~20 atoms, cluster intensities drop off roughly exponentially with increasing size for all charge states. Note the presence of large gold clusters (Au_x)—extending to 100, 90, and 150 atoms for singly charged anions, cations, and neutrals, respectively (Table 1). These are the largest clusters so far detected on simple laser ablation of metal targets in high vacuum. Superimposed on the monoanion series is a set of peaks caused by dianions (extending to even larger sizes), which we will return to below.

For the same incident ion velocities (but charge-state optimized extraction—see Experimental), detector signal levels were roughly the same for prompt cation and anion clusters of the same nuclearity. In the absence of absolute one (and multi)-photon ionization cross sections for gold clusters, the ratio of neutral to charged particles emitted from the ablation target cannot be accurately quantified. As a rough measure, based on ionization photon flux, theoretical assessments of near-threshold photoionization cross sections in simple metal clusters [20], as well as the relative ion yields observed for prompt versus postionized cations, only a few percent of the ablated particles are emitted as ions.

The relative intensities of promptly formed gold monoanion and monocation clusters show prominent even–odd effects in the size range of up to ~20 atoms. At the same time, we also observe weak jellium shell structure for both charge states indicative of ion stability islands (e.g., drops in intensity after

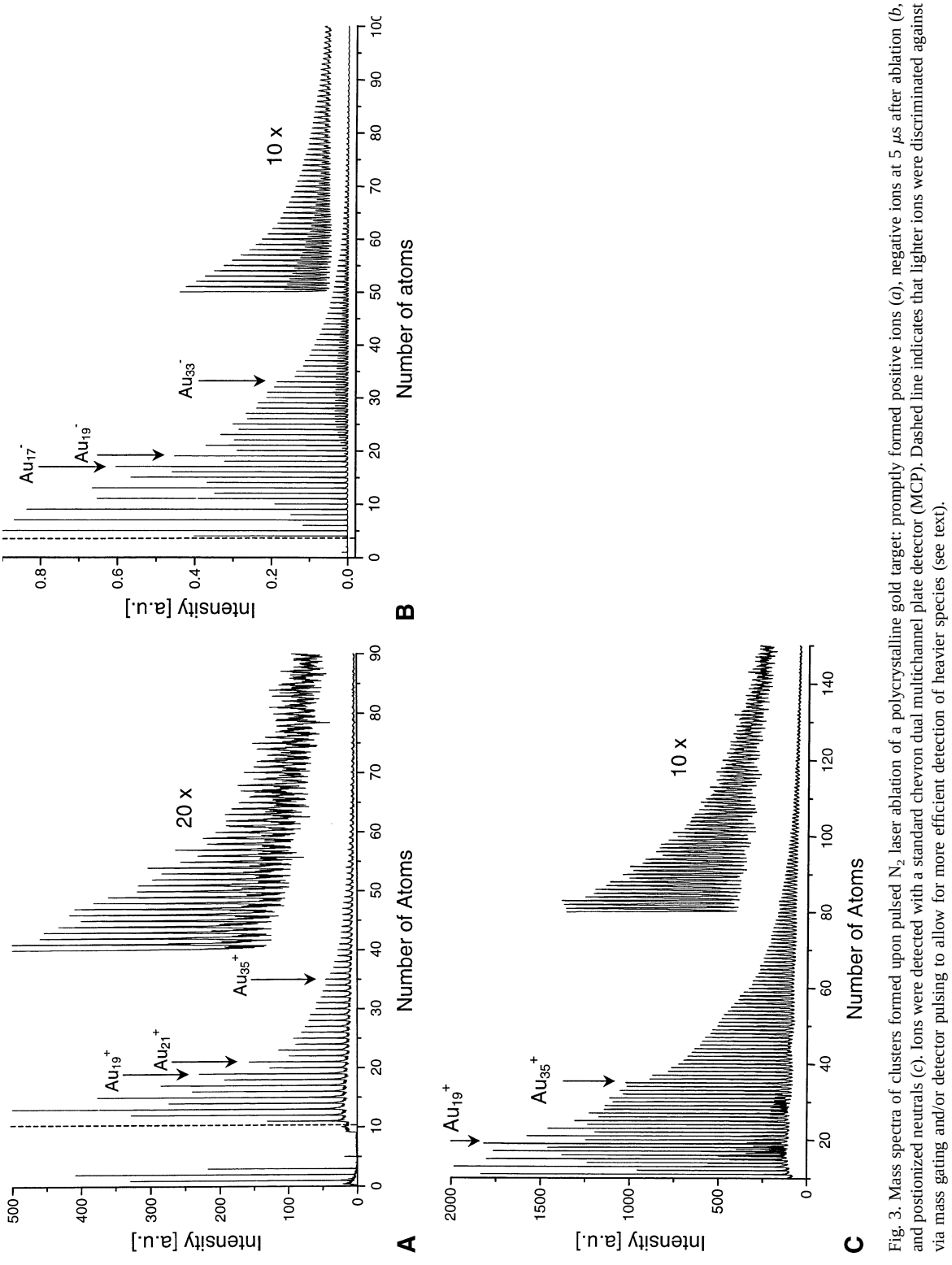

Fig. 3. Mass spectra of clusters formed upon pulsed N_2 laser ablation of a polycrystalline gold target: promptly formed positive ions (*a*), negative ions at 5 μs after ablation (*b*, and postionized neutrals (*c*). Ions were detected with a standard chevron dual multichannel plate detector (MCP). Dashed line indicates that lighter ions were discriminated against via mass gating and/or detector pulsing to allow for more efficient detection of heavier species (see text).

Table 1
Detected Cluster Size Ranges

Target	Monocations	Neutrals[a]	Monoanions	Dianions	Trianions
Au	1–90	1–150	1–100	29–200	· – ·
Pb	1–6	1–12	1–100	35–200	76–200
Pt	1–3	1–3	1–60	· – ·	· – ·
Sb	· – ·	· – ·	1–45	[b]	· – ·
Bi	1–4	1–3	1–33	· – ·	· – ·

Note. Ranges shown for each element studied are the cluster sizes detected mass spectroscopically—as a function of charge state—see text for details

[a] Postionized with an ArF laser.

[b] Inconclusive measurements.

Au_{19}^- and Au_{33}^-) [21]. The positive ion mass spectra recorded for postionized neutrals under one-photon ionization conditions also manifest such abundance discontinuities with jellium shell structure apparent to even larger cluster sizes.

A number of experiments were performed to test ion source stability. Sequential mass spectra obtained over periods of >4 h at nominally constant ablation and detection conditions (typically 1000 pulses per mass spectrum at 10 Hz) showed that the intense signals associated with small clusters ($x < 5$; all charge states) are stable to within 15%–20%—as long as the target was rotated. The signal intensity fluctuation of larger clusters was more pronounced but not studied in detail.

To gauge the absolute intensity of the cluster (ion) source, we also recorded anion mass spectra using a calibrated charge sensitive detector (CSD). This type of detector is slower and less sensitive than an MCP detector but has the advantage of being insensitive to incident momentum and, therefore, not cluster size dependent in its response (at least to first order and as long as all secondary charged particles emitted following ion impact can be deflected back to the detector active area). Fig. 4 contains a negative ion mass spectrum recorded with the CSD under the same

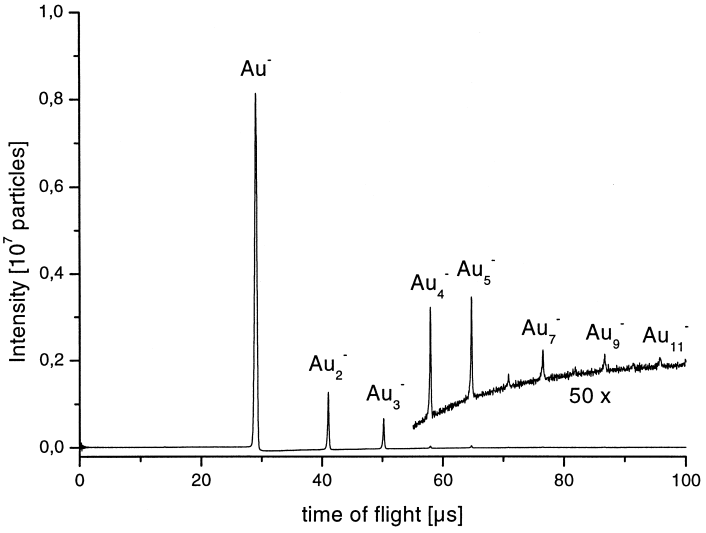

Fig. 4. Mass spectra of negative ions formed under the same conditions as in Fig. 3 but detected with a charge-sensitive detector (CSD). *Y*-axis corresponds to the total ion yield per laser shot [39].

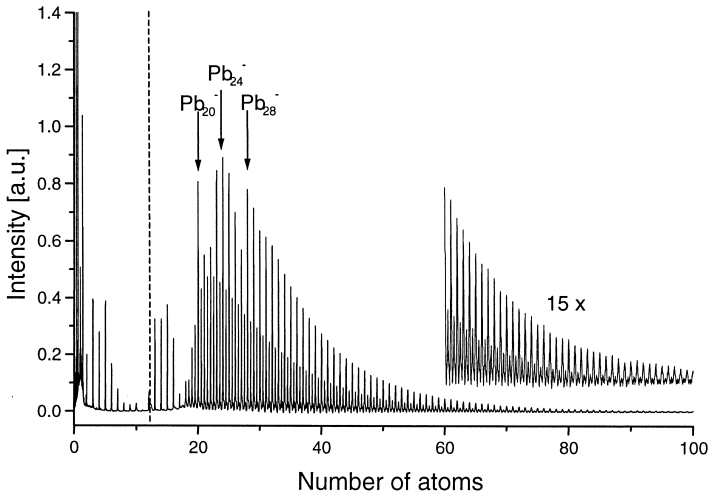

Fig. 5. Mass spectra of directly formed negative ions generated on pulsed laser ablation of a lead target (see text for details). Ions were detected with an MCP detector. Dashed line as in Fig. 3.

ablation conditions as in Fig. 3 (but without mass gate discrimination (no saturation issue as with an MCP). The largest anion detectable under optimized conditions was Au_{11}^-, for which we observed an average single shot ion current of 10^{-15} C. This translates to a lower limit of 7000 Au_{11}^- produced per laser pulse (after taking into account 10% grid loss). Note that ion trajectory simulations and measurements with a position-sensitive MCP detector [22] indicate that under the conditions of our experiment, essentially all laser-generated Au_{11}^- are directed toward the CSD active surface.

Singly negatively charged species larger than $x = 11$ were not detectable with the CSD. Nevertheless, a lower limit to their absolute yield may be obtained by both calibrating the MCP detector against CSD signal at Au_{11}^- and assuming the MCP response is size independent (it is actually thought to be proportional to incident velocity for a specific cluster size and proportional to monomer count for a series of clusters having the same [above secondary electron emission threshold] incident velocities [23]). We then surmise from the anion mass spectrum in Fig. 3 that gold clusters at the top end of the mass range are $\sim 5 \times 10^5$ times less likely to be formed than an atomic or dimer anion (i.e., at least 30 such cluster species per laser pulse). This ratio then also provides a rough indication of the dynamic range of our mass spectrometer.

3.1.2. Lead and other metals

Under analogous irradiation conditions, large cluster monoanions (M_x^-, $x > 30$) were observed for a variety of other metal targets, notably lead, bismuth, antimony, and platinum. In contrast to gold, anion yields for all metals were always significantly larger than cation yields (and the cluster size ranges associated with anions were correspondingly larger). Table 1 summarizes cluster size ranges observed as a function of charge state. In addition to the elements tabulated, we also attempted to generate clusters of Na, Mg, Ag, and Cd with the same approach. For these elements, only atoms, dimers, and traces of clusters with fewer than five atoms were observed (in all charge states probed).

Of the elements probed, by far the strongest direct cluster ion signals and the largest observable clusters were obtained for lead targets (excepting gold). Fig. 5 shows the corresponding anion mass spectrum. A prominent Pb_x^- series is recognizable, which within our mass resolution, appears to extend up to $x = 100$. This series shows pronounced abundance discontinuities in the small cluster size range dropping off to a minimum at $x = 17$. While a local abundance

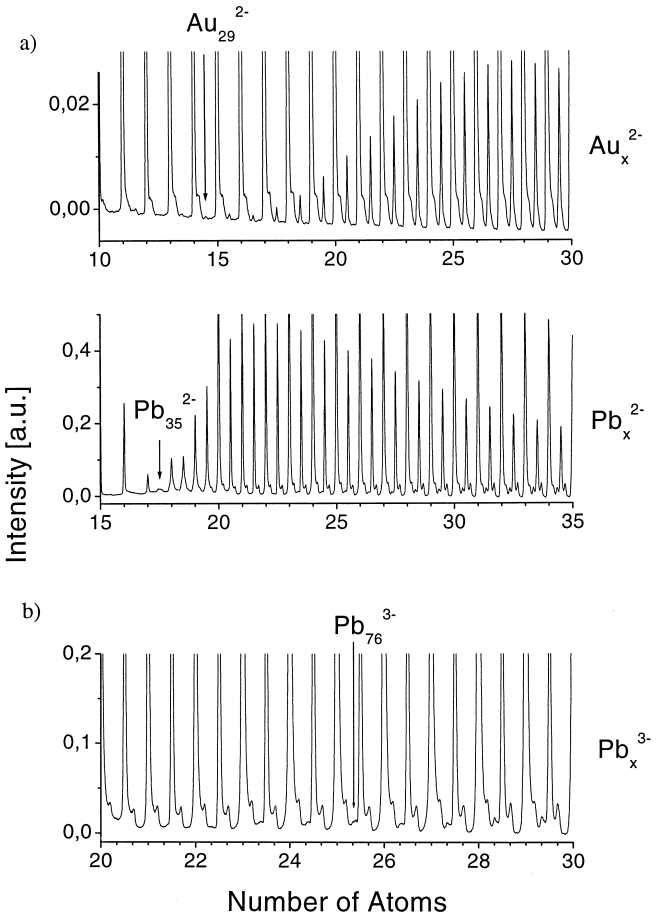

Fig. 6. (*a*) expanded scale blowup of the dianion threshold regions for gold (Fig. 2) and lead (Fig. 4) measurements; (*b*): expanded scale blow-up of the trianion threshold region for lead (Fig. 4, see text).

maximum at Pb_{15}^- has been observed for clusters generated with a PACIS source [24], there are no comparable mass spectra in the literature. Above $x = 17$, Fig. 5 shows evidence for doubly negatively charged lead clusters.

3.2. Multianions

3.2.1. Dianions

Among the elements probed in this study, a contiguous series of cluster dianions M_x^{2-} were seen for both gold and lead targets (see Table 1). Both series commence at characteristic threshold sizes of $x = 29$ and 35, respectively. Fig. 6a shows blowups of the corresponding threshold regions. Relative dianion signal (compared with monoanions of the same nuclearity) was significantly larger in the case of lead targets. Dianions were not unequivocally observed for any of the other metal targets studied. Size-dependent trends in dianion yield can only be surveyed at odd nuclearities x ($m/z = xM$[Pb,Au]/2, where M corresponds to the respective atomic mass), where signals are not perturbed by superimposed singly charged species. For both metals, the corresponding odd-nuclearity dianion sequence builds up from background noise to maximal signal levels within a range of 15–20 atoms.

The mass spectra shown in Figs. 3, 5, and 6 are

typical with regard to onset regions—within the small range of laser fluence variation that still yields sufficient signal-to-noise ratio. However, accurately defining the onset size is in both cases complicated by small amounts of contaminant ions in the prethreshold regions, which occur just below half integral cluster nuclearity. Therefore, our assigned threshold sizes, corresponding to the smallest dianions to be unequivocally observed with a signal-to-noise ratio ≥ 2 are to be regarded as upper limits.

Dianions are detected more efficiently than monoanions of the same nuclearity because they are significantly faster. In addition, for two ions at the same *m/z* (and same velocity), the more highly charged cluster will be detected more efficiently, as it is comprised of the larger number of atoms [23]. Consequently, the robust dianion signals observed at odd nuclearity are in part because of enhanced detection efficiency of the MCP for such species. Nevertheless, in particular for lead clusters, relative dianion yields must be quite large. Here, odd-nuclearity lead-cluster dianion signals track roughly with the adjacent integral intensities (suggesting that the latter are comprised dominantly of even x dianion signals together with only small amounts of $x/2$ monoanions).

Dianion mass spectral peak shapes (Figs. 6 and 7) appear significantly broadened near size thresholds. This argues for significant metastable decay on the extraction time scale. To obtain further information on the metastable decay of lead cluster dianions on the time scale of their passage through the TOFMS drift tube ($\sim$5.5–60 μs after ablation), a series of mass spectra were recorded with various mass gate-blocking potentials applied (Fig. 7). Note that under these measurement conditions, parent dianions are thrown out to within $>$99.9% at deflection voltages of 360 V and above. Full deflection of any monoanions resulting from in-flight electron autodetachment requires a blocking voltage of $>$720 V. This also represents the voltage required to shield the detector from all possible charged fragments at the parent dianion velocity—as lighter singly charged fragment ions moving at the parent dianion velocity require lower blocking voltages. Neutral fragmentation products will, of course, be uninfluenced by the mass gate.

The 800-V measurement of Fig. 7 was then carried out under conditions for which only neutral dianion fragments (and very small amounts of autodetached [di$>$mono]anions) can hit the detector. The measurement indicates detectable signals ($<$5% of the parent ion intensity) for all $m/z = yM$(Pb) ($y\in$ positive integer) over the range probed. In contrast, there was generally little or no signal apparent at $m/z =$ yM(Pb)/2 with one exception: $y = 37$ just above the dianion size threshold. The implications of these observations will be discussed below.

3.2.2. Trianions

Fig. 6a and 6b show that ion peaks at long flight times manifest a small shoulder to higher mass that scales in intensity approximately with the primary peak. This is likely an instrumental artifact associated with anion detection. Taking this into account, Fig. 6b, which contains a blow-up of Fig. 5 in the *m/z* range 4140–6210, indicates a series of lead cluster trianions. In particular, two slowly rising peak series at nominally third integral nuclearities are apparent (M_x^{3-} for $x = [3y + 1]M[\mathrm{Pb}]/3$ and $[3y + 2]M[\mathrm{Pb}]/3$, where $y\in$ positive integer). The $3y + 1$ series is superimposed on the unresolved shoulder of the y monoanion ($+2y$ dianion). The corresponding trianion threshold size lies at roughly 76. Again, this is an upper limit. Within the signal-to-noise constraints of our setup, we did not observe metal cluster trianions for any of the other metals studied.

4. Discussion

4.1. Mechanism for cluster formation

There is an extensive literature on the interaction of pulsed laser beams with metal surfaces under vacuum conditions [25]. Apart from clusters, one often observes ejected droplets of various sizes. These are typically detected by deposition followed by scanning electron microscopy (SEM) and range in size from particles at the resolution limit of the SEM to micron-sized objects (assuming that deposition is not associated with aggregation). Droplets are obvi-

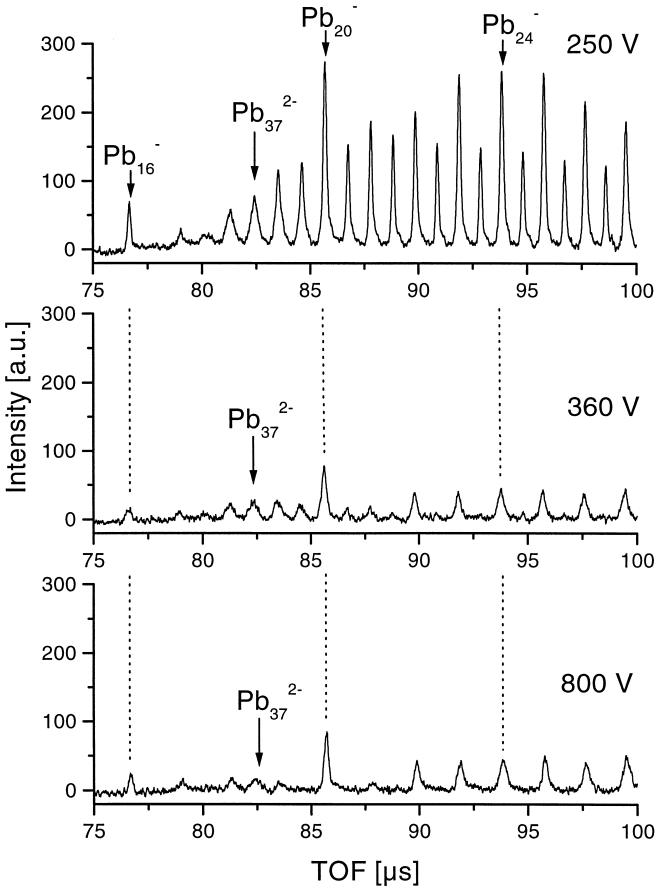

Fig. 7. Partial lead-cluster anion mass spectra as a function of the mass, gate-blocking potential. The potential was applied throughout the time-window shown (see text).

ously detrimental to uniform thin-layer formation via laser ablation [26] as well as to spatially resolved elemental analysis of ablation targets [27]—two important applications of laser ablation as applied to metal surfaces. Droplet formation has therefore been studied in some detail—much more extensively than (intermediate-sized) cluster generation about which little is known in this context. Droplets are thought to be formed either via subsurface boiling or hydrodynamic sputtering [25,26]—each involving the temporary formation of liquid regions at or within the target surface.

One can speculate that clusters derive from the same mechanism as droplets—that is, are not generated by gas-phase aggregation. In this context, it is of interest to note that scanning electron microscopy of several multipulse-ablated gold targets used in this study reveals spheroidal surface structures of diameter between 10 and 100 nm. As an example, Fig. 8 shows a representative SEM image of the gold target that was used to obtain the mass spectra shown in Fig. 3 (subsequent to mass spectral acquisition). The presence within the spheroidal structures of circular or oval openings much as in burst bubbles frozen at the moment of their rupture is consistent with cluster formation via local melting and boiling. We note in passing that similar SEM images were obtained for targets ablated without an applied electric field.

In using a 500-ps N_2 ablation laser, we have observed significant cluster yields preferentially for

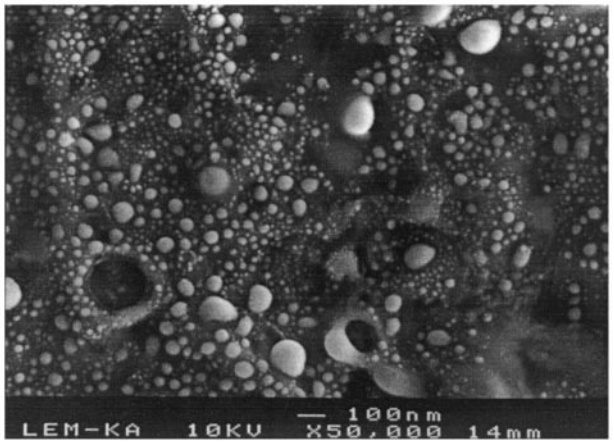

Fig. 8. SEM image of the gold target used for Fig. 3 following laser ablation (10^5 pulses).

heavy atom targets. Assuming subsurface boiling is responsible, the extent of clustering under our laser ablation conditions must clearly be a complex function of the optical and thermal properties of the target material (both solid and liquid) as well as of its time-dependent surface morphology. An in-depth analysis of both aspects is beyond the scope of this study. The charged-particle yield is even more intractable. This will depend on both the electronic structure of the molten target, charge transfer dynamics [28], and the optical and electronic properties of the major constituents of the vapor/plasma plume. In future systematic work, it will be of interest to probe for wavelength and pulse length dependence of cluster formation.

4.2. Threshold sizes for multianions

Dianion onsets were observed at $x = 29$ and 35 for gold and lead clusters, respectively. How do these threshold sizes arise, and do they provide intrinsic electronic structure information on the clusters involved?

Interestingly, Au_{12}^{2-}, a dianion much smaller than the size threshold found in this study, has been generated and stored on the second time scale in a Penning ion trap [12]. What is the explanation for this difference? The study by Schweikhard et al. was carried out with gold cluster anions thermalized to near room temperature. Three observations suggest that our gold clusters exit in the ablation plume with much higher internal excitations [19]. Photodetachment spectroscopic probes of Au_3^- generated under identical conditions are consistent with a vibrational temperature >2000 K—5 μs after formation. Neutral particle velocity distributions (which were measured for $x = 1$ and 2) can be interpreted as indicating even higher translational temperatures. The mass spectral peak broadening associated with gold cluster dianion signals near the size threshold (Fig. 6) is also consistent with high internal excitation levels, as it suggests that metastable decay is still ongoing on the extraction time scale for quite large clusters.

Consequently, in discussing dianion threshold sizes in our experiment, it is first of interest to consider all energetically possible metastable decay channels. Depending on element and cluster size these are: electron autodetachment, fragment monoanion loss, and neutral fragment loss (Eqq. [1–3]).

$$M_x^{2-} \rightarrow M_x^- + e^-, \quad (1)$$

$$M_x^{2-} \rightarrow M_{x-y}^- + M_y^-, \quad (2)$$

$$M_x^{2-} \rightarrow M_{x-y}^{2-} + M_y. \quad (3)$$

Dissociation into two clusters ($y > 3$; monoanion/monoanion and dianion/neutral) is not expected to play an important role on energetic grounds, except perhaps for monoanion fragment pairs with particularly high first-electron affinities [29]. Reaction (3) cannot play a role in determining dianion thresholds (because a smaller dianion would result). Then either electron autodetachment or loss of a small monoanion (presumably atom or trimer, which for gold, have first electron affinities of 2.31 and 3.8 vs. 1.94 eV for the dimer [30]) are responsible. What are the respective activation energies?

According to a classical electrostatic approach [31], the *n*th electron affinity of a metal sphere of radius R is given by Eq. (4), (where WF corresponds to the bulk polycrystalline work function: 5.31 and 4.25 eV for gold and lead, respectively and $R = r_M x^{1/3}$, where r_M is an effective atomic radius based on tabulated bulk densities, [32]).

$$\mathrm{EA}(n) = \mathrm{WF} - [(2n-1)/2](e^2/4\pi\varepsilon_0 R) \quad (4)$$

Inserting $r_{\mathrm{Au}} = 159$ pm and $r_{\mathrm{Pb}} = 193$ pm, one can calculate that the smallest gold cluster to have a positive second electron affinity is $x = 17$ ($x = 18$ for lead). Our threshold sizes lie significantly above these numbers because there are two further issues. In this small cluster-size range, experimental EA(1) values can deviate significantly from the classical electrostatic prediction (basically as a result of nonspherical symmetries and quantum size effects) [33]. One would expect second electron affinities, which are not known experimentally, to be even more strongly off. A recent semiempirical assessment, in fact, predicts that already Au_{15}^{2-} has a positive electron binding energy (second electron affinity; EA (2)) [12]. Extrapolating this prediction to our threshold size, we would expect an EA(2) of ~1.0 eV for $x = 29$.

Classically, electron autodetachment from a multianion with n excess electrons requires more energy than EA(n) because an intervening Coulomb potential barrier must also be surmounted. This may be calculated from the barrier that is encountered in adding an electron to an anion with $(n-1)e$ charges. The required energy can be approximated in terms of the classical electrostatics of further charging a charged metallic sphere [34]. The Coulomb interaction between a negatively charged metal sphere of radius R (and charge $[n-1]e$) and a negative point charge e at $r > R$ from the sphere center is then given by Eq. (5):

$$E_B(r) = (e^2/4\pi\varepsilon_0 R)\,[(n-1)\,R/r + R^2/2r^2 - R^2/2(r^2 - R^2)]. \quad (5)$$

The corresponding function manifests a maximum at $r_{\max}(n-1)$—the Coulomb barrier height relative to the outside infinite separation limit. For $n = 2$, evaluating $dE_B/dr = 0$ yields, $r_{\max} = 1.62R$ and $E_B(r_{\max}) = (e^2/8\pi\varepsilon_0 R)$. Consequently, for gold cluster monoanions in the size range of $x = 20$–40, one obtains a barrier of 1.67–1.32 eV to electron addition. The corresponding barrier to electron autodetachment is calculated by summing $E_B(r_{\max})$ and EA(2).

For our threshold size, we would consequently expect that an activation energy of $1 + 1.5 = 2.5$ eV (corresponding to EA(2) + $E_B[r_{\max}]$ = WF − $e^2/4\pi\epsilon_0 R$) is required for classical autodetachment to the monoanion. This neglects electron tunneling, which allows for electron loss at less than the classical threshold energy (not a large effect on our short experimental time scale). Note that on the basis of Eqq. (4) and (5), the activation energy for electron autodetachment drops to near 2.0 eV as dianion size is reduced from $x = 29$ to $x = 20$.

A rough assessment using a liquid drop model to approximate the stability of spherical dianionic gold clusters [35] indicates that the Au evaporation energy from Au_x^{2-} (reaction (3), $y = 1$) remains near 3 eV throughout the size range of interest. Consequently, electron loss will prevail energetically over evaporation below about $x = 30$. The liquid drop model may also be applied to fission processes. Here, assumptions concerning the barrier configuration are additionally required. For this, we make use of calculations for multiply positively charged metal clusters, which have been extensively studied because of strong analogies between their fragmentation physics and those of atomic nuclei [35,36] (ignoring the issue

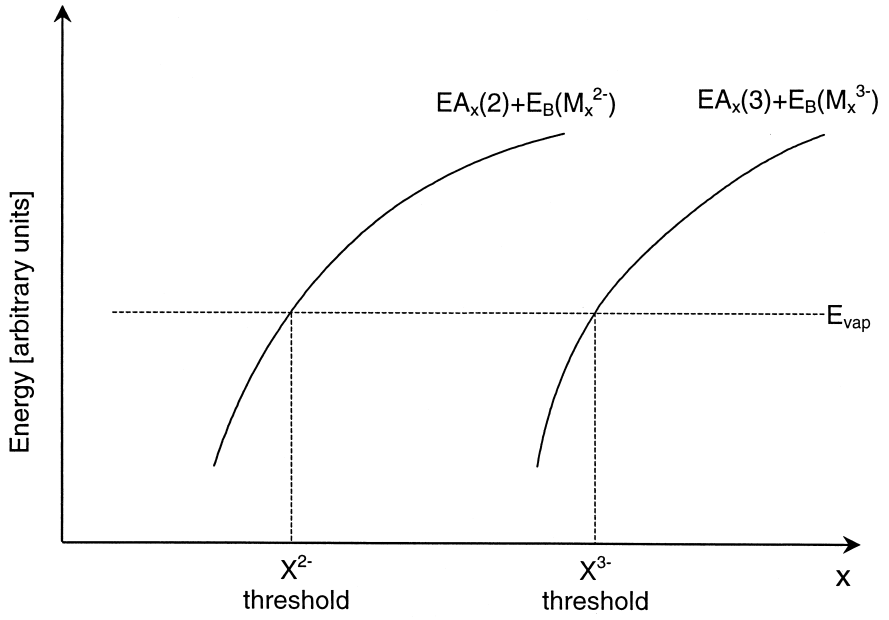

Fig. 9. Schematic representation of decay energetics for metal cluster dianions and trianions. Atom evaporation energies are roughly size independent (dashed line). Autodetachment activation energies comprise the nth electron affinity (EA(n), Eq. [4]). plus the corresponding Coulomb barrier (E_B, Eq. [5]) and are strongly size dependent (continuous lines). Electron loss prevails below the respective crossing points. Fission energies are assumed to be too high to compete.

of stronger polarization interaction associated with nascent monoanionic fragments on top of the fission barriers). A rough calculation analogous to that for gold dications [37] indicates that asymmetric fission into two monoanions requires less activation energy the smaller the cluster is and that the corresponding fission activation energy also eventually drops below the 3 eV Au evaporation energy line.

Consequently, for large dianions we would expect evaporation to be the energetically most favorable decay channel. For sufficiently small species, both electron loss and asymmetric fission require less energy than evaporation. Given an evaporative ensemble of hot dianions, both channels would lead to a low mass cutoff in the dianion mass spectral series. Note that dication threshold sizes observed on high-energy electron impact (EI) or multiphoton ionization (MPI) of neutral metal cluster beams have been analogously rationalized in terms of a cluster size–dependent transition from evaporative to fission decay [38]. For gold, a 150 eV EI dication threshold of $x = 14$ has recently been observed, somewhat smaller than the $x = 29$ seen here for dianions [37]. This may argue for the prevalence of electron loss processes (1) rather than asymmetric fission (2) as threshold determining in our case.

We then propose the following explanation for our observations (schematically represented in Fig. 9). Laser ablation gives rise to a wide size range of very hot mono- and dianions, initially also including dianions below the observed size threshold. Metastable decay immediately sets in and preferentially follows the energetically most favorable channel. The first several decay steps are always much faster than the extraction time scale. Consequently, below-threshold dianions are immediately lost from the dianion into the monoanion charge state. In contrast, above-threshold dianions may be replenished by preferential Au evaporative decay from larger dianions. This is indicated schematically by the reaction sequence (6):

$$Au_{34}^{2-} \rightarrow\rightarrow Au_{29}^{2-} \rightarrow Au_{29}^{-} + e^{-} \quad (6)$$

The threshold sizes observed for lead cluster dianions may be similarly rationalized. The mass gate-blocking experiments of Fig. 7 provide further support. Above the $x = 35$ threshold, dianions decay by Pb evaporation into easily deflectable dianions (the associated undeflected fast Pb atoms are inefficiently detected). Consequently, there is little or no signal at half-integral nuclearity masses for deflection voltages $\geq$360 V. Near threshold, decay into monoanions by electron autodetachment begins to occur (cf. sequence [6]). The corresponding signals, in particular $x = 37$, are therefore persistent to higher blocking voltages.

In fact, Fig. 7 is consistent with (further) decay of monoanions into readily detectable fast neutral clusters. This appears to be a prominent decay channel for monoanions throughout the size range of interest. The surprisingly high relative dianion abundance in Fig. 5, then, likely reflects evaporative retention of the dianion charge state until the clusters have fragmented down to $x \approx 35$. In contrast, hot singly charged species are efficiently lost to the neutral channel for all x probed.

Above, we have argued that for Pb_{35}^{2-}, the Pb evaporation energy is equal to the sum of EA(2) and Coulomb barrier to electron loss (autodetachment activation energy). This is calculated to be 2.0 eV. For trianions, we can similarly argue that the observed threshold size represents the cluster size at which the autodetachment activation energy is equal to the Pb evaporation energy. Differentiating Eq. (5) and solving for r_{max} ($n = 3$), the outside barrier height for electron loss is calculated to be $1.165e^2/4\pi\varepsilon_0 R$. Adding to this the electron affinity according to Eq. (4) (EA (3)), one obtains an ionization activation energy of WF-$1.335e^2/4\pi\epsilon_0 R$. Inserting $x = 76$ and the effective atomic radius of 193 pm, we obtain a trianion Pb evaporation energy of 1.9 eV. This is in fair agreement with the dianion evaporation energy as one would expect for a large cluster—arguing for electron autodetachment as the lower-energy threshold-defining channel (as opposed to scission) for trianions also.

5. Summary

Pulsed laser ablation of gold, lead, platinum, bismuth, and antimony surfaces under high vacuum conditions is shown to lead to the formation of significant amounts of unexpectedly large clusters in several charge states—primarily neutral. The mechanism of cluster formation presumably involves (sub) surface melting and explosive ejection of multiple droplets in a wide size distribution. In the case of gold targets, neutral clusters as large as 150 atoms were observed—significantly larger than previously detected under comparable conditions. This is a consequence of our detection setup, which encompassed a linear time-of-flight mass spectrometer designed for large dynamic range and high detection sensitivity.

In addition to neutral, singly positively, and negatively charged clusters, the material ablated from gold and lead targets contains measurable amounts of dianion clusters (as well as trianions for lead). There is only one previous report of metal cluster multianion formation [12,14]. This was accomplished via electron pick-up onto preformed monoanion clusters in a room-temperature Penning trap. The surprisingly simple multianion source presented here should facilitate spectroscopic studies of such species in pulsed ion beams.

For both gold and lead clusters, dianion series extended out to species with >200 atoms. Associated with both series were size thresholds at $x = 29$ and 35 (Au and Pb, respectively), below which dianions could not be observed. These threshold sizes can be rationalized in terms of an ensemble of preformed hot dianions that undergo metastable decay via either neutral atom evaporation or electron autodetachment—before ion extraction. Below threshold, decay channels leading to monoanions prevail. Above threshold, neutral atom evaporation to smaller dianions is thermodynamically preferred. The trianion threshold observed for Pb may be similarly rationalized.

In the future, it will be of interest to gauge the reasons for pronounced element specificity in both cluster formation as well as multianion yield. A further unresolved issue is the apparent absence of

multications in both the lead and gold cluster systems, whereas multianions can be readily observed. Such charge asymmetry may reflect tunneling electron-transfer dynamics close to the surface.

Acknowledgments

This research was supported by the Deutsche Forschungsgemeinschaft under SFB 195, Lokalisierung von Elektronen in Makroskopischen und Mikroskopischen Systemen. We thank F. Hillenkamp and his group for help in constructing the CSD.

References

[1] See, for example: C. Jin, R. Hettich, R. Compton, A. Tuinman, A. Dereskei-Kovacs, D. Marynick, B. Dunlap, Phys. Rev. Lett., 73, (1994) 2821; R. Compton, A. Tuinman, C. Klots, M. Pederson, D. Patton, Phys. Rev. Lett. 78 (1997) 4367; X. Wang, L. Wang, J. Chem. Phys. 111 (1999) 4497; L. Wang, C. Ding, X. Wang, S. Barlow, Rev. Sci. Instr. 70 (1999) 1957; X. Wang, L. Wang, Nature 400 (1999) 245.
[2] X. Wang, L. Wang, Phys. Rev. Lett. 83 (1999) 3402.
[3] P. Weis, O. Hampe, S. Gilb, M. Kappes, Chem. Phys. Lett. 321 (2000) 426.
[4] J. Friedrich, P. Weis, J. Kaller, R. Whetten, M. Kappes, Eur. J. Phys. D 9 (1999) 269.
[5] M.E. Geusic, M.D. Morse, S.C. O'Brian, R.E. Smalley, Rev. Sci. Instrum. 56 (1985) 2123.
[6] H. Siekmann, C. Lüder, J. Faehrmann, H. Lutz, K.-H. Meiwes-Broer, Z. Phys. D 20 (1991) 417.
[7] K. Sattler, J. Mühlbach, E. Recknagel, Phys. Rev. Lett. 45 (1980) 821.
[8] K. Leiter, W. Ritter, A. Stamatovic, T. Märk, Int. J. Mass Spectrom. Ion Proc. 68 (1986) 341.
[9] S. Schauer, P. Williams, R. Compton, Phys. Rev. Lett. 65 (1990) 625.
[10] P. Limbach, L. Schweickhard, K. Cowen, M. McDermott, A. Marshall, J. Coe, J. Am. Chem. Soc. 113 (1991) 6795.
[11] R. Hettich, R. Compton, R. Ritchie, Phys. Rev. Lett. 67 (1991) 1292.
[12] A. Herlert, S. Krückeberg, L. Schweikhard, M. Vogel, C. Walther, Physica Scripta T80 (1999) 200.
[13] L. Schweikhard, A. Herlert, S. Krückeberg, M. Vogel, C. Walther, Philosophical Mag. B 79 (1999) 1343.
[14] A. Herlert, K. Hansen, L. Schweikhard, M. Vogel, Hyperfine Interactions, in press 127 (2000) 529.
[15] R. Hettich, J. Am. Chem. Soc. 111 (1989) 8582.
[16] H. Kim, T. Wood, A. Marshall, J. Lee, Chem. Phys. Lett. 224 (1994) 589.
[17] C. Stoermer, S. Gilb, J. Friedrich, D. Schooss, M. Kappes, Rev. Sci. Instr., 69, (1998) 1661.
[18] U. Bahr, U. Röhling, C. Lautz, K. Strupat, M. Schürenberg, F. Hillenkamp, Int. J. Mass Spectrom. Ion Processes Processes (1996) 9.
[19] R. Wesendrup, T. Hunt, P. Schwerdtfeger, J. Chem. Phys. 112 (2000) 9356; and references therein.
[20] K. Koskinen, M. Manninen, Phys. Rev. B 54 (1996) 14796.
[21] See, for example, M. Kappes, Chem. Rev. 88 (1988) 369; W. de Heer, Rev. Mod. Phys. 65 (1993) 611.
[22] Carsten Stoermer, Ph.D. Thesis, University of Karlsruhe, 2000.
[23] See, for example, M. Kappes, S. Leutwyler, in: Atomic and Molecular Beam Methods (G. Scoles, Ed.), Vol 1, Oxford University Press, Oxford, 1988, p. 405.
[24] C. Lüder, K. Meiwes-Broer, Chem. Phys. Lett. 294 (1998) 391; references therein.
[25] See, for example, R. Russo, Appl. Spectroscopy, 49, (1995) 14A; M. von Allmen, A. Blatter, Laser Beam Interactions with Matter, Springer Series in Material Science, Vol. 2, Springer, Berlin, 1995.
[26] D. Chrisey, G. Hubler (Eds.) Pulsed Laser Deposition of Thin Films, Wiley, New York, 1994.
[27] Y. Huang, Y. Shibata, M. Morita, Anal. Chem. 65 (1993) 2999.
[28] M. Hillenkamp, J. Pfister, M. Kappes, to be published.
[29] C. Yannouleas, U. Landman, Phys. Rev. B 61 (2000) R10587.
[30] J. Hoe, K. Ervin, W. Lineberger, J. Chem. Phys. 93 (1990) 6987.
[31] D. Wood, Phys. Rev. Lett. 46 (1981) 749; M. Seidl, J. Perdew, Phys. Rev. B 50 (1994) 5744.
[32] D. Lide (Ed.), CRC Handbook of Chemistry and Physics, 71st ed., CRC Press, Boca Raton, FL, 1990.
[33] M. Seidl, K.-H. Meiwes-Broer, M. Brack, J. Chem. Phys. 95 (1991) 1295.
[34] J. Jackson, Classical Electrodynamics, 3rd ed., Wiley, New York, 1998.
[35] U. Näher, S. Bjornholm, S. Frauendorf, F. Garcias, C. Guet, Phys. Rep. 285 (1997) 245.
[36] C. Brechignac, P. Cahuzac, F. Carlier, M. de Frutos, N. Kebaili, J. Leygnier, A. Sarfati, V. Akulin in: T. Martin (Ed.) Large Clusters of Atoms and Molecules, Kluwer, Dordrecht, 1996; C. Brechignac, P. Cahuzac, N. Kebaili, J. Leygnier, Phys. Rev. Lett. 81 (1998) 4612.
[37] J. Ziegler, G. Dietrich, S. Krückeberg, K. Lützenkirchen, L. Schweikhard, C. Walther, Hyperfine Interactions 115 (1998) 171.
[38] See, for example; S. Krückeberg, G. Dietrich, K. Lützenkirchen, L. Schweikhard, C. Walther, J. Ziegler, Eur. Phys. J. D. 9 (1999) 169.
[39] The rising baseline is an electronic artefact caused by the high monomer signal.